Atmospheric Research 188 (2017) 39–47

Contents lists available at ScienceDirect

Atmospheric Research

journal homepage: www.elsevier.com/locate/atmosres

Aerosol optical properties at urban and coastal sites in Shandong Province, Northern China

Weida Yan [a], Lingxiao Yang [a,b,c,*], Jianmin Chen [a,b,c,d], Xinfeng Wang [a], Liang Wen [a], Tong Zhao [a], Wenxing Wang [a]

[a] Environment Research Institute, Shandong University, Jinan 250100, China
[b] School of Environmental Science and Engineering, Shandong University, Jinan 250100, China
[c] Jiangsu Collaborative Innovation Center for Climate Change, China
[d] Shanghai Key Laboratory of Atmospheric Particle Pollution and Prevention (LAP3), Fudan Tyndall Centre, Department of Environmental Science and Engineering, Fudan University, Shanghai 200433, China

ARTICLE INFO

Article history:
Received 13 September 2016
Received in revised form 15 December 2016
Accepted 27 December 2016
Available online 29 December 2016

Keywords:
Aerosol optical properties
Diurnal cycle
Wind direction and speed

ABSTRACT

In-situ observations of aerosol optical properties were conducted in Jinan, an urban site, from December 2013 to May 2014 and on Tuoji Island, a coastal site, from December 2014 to January 2015; both locations are located in Shandong Province, Northern China. Aerosol optical properties, such as the scattering coefficient (σ_{sp}), absorption coefficient (σ_{ap}) and single-scattering albedo (ω), were obtained using nephelometer and aethalometer. The mean values ($\pm$standard deviation) for σ_{sp} at 550 nm and σ_{ap} at 532 nm, were 204 $\pm$ 188 Mm^{-1} and 43 $\pm$ 33 Mm^{-1}, respectively, in Jinan and 210 $\pm$ 246 Mm^{-1} and 8 $\pm$ 6 Mm^{-1} on Tuoji Island, respectively. The average ω at 532 nm was 0.80 $\pm$ 0.09 in Jinan and 0.93 $\pm$ 0.04 on Tuoji Island. Pronounced diurnal cycles were observed at both locations for σ_{sp}, σ_{ap} and ω, but the diurnal cycles at the two locations exhibited distinct properties for some of the aerosol optical parameters. The values of σ_{sp} and σ_{ap} peaked between 0800 and 1100 local time (LT) due to traffic emissions and low wind speeds at both locations. And a unimodal ω diurnal cycle, which peaked between 1000 and 1400 LT, was observed in the spring in Jinan. This spring diurnal pattern was mainly related to secondary aerosol formation and aging processes. The high σ_{sp} and σ_{ap} values in Jinan winter were accompanied by calm winds (<2 m/s) from 0° to 90°, while the high σ_{sp} and σ_{ap} values on Tuoji Island were observed during the period of stronger wind speeds (>2 m/s) from 180° to 270°. This indicates that local emissions were a key source of strongly absorbing and scattering aerosols in Jinan during heating period, whereas, high σ_{sp} and σ_{ap} values on Tuoji Island were mainly influenced by middle- and long-distance transport from Shandong Province and the Jing-Jin-Ji region. Additionally, middle- and long-distance regional transport from direction at 180° to 270° occasionally enhanced the σ_{sp} and σ_{ap} values in the spring at Jinan after heating period. The σ_{sp} values in Jinan and Tuoji Island both exhibited relatively profound correlation with the accumulation-mode particle number concentrations.

1. Introduction

It is generally accepted that atmospheric aerosol particles are among the most variable components of the Earth's atmosphere and that they can significantly affect the Earth's energy budget (Forster et al., 2010; Haywood and Shine, 1997; IPCC, 2013; Ma et al., 2011). Not only can they directly scatter and absorb incoming and outgoing solar and terrestrial radiation, but they can indirectly enhance cloud reflectivity by acting as cloud condensation nuclei (Kaufman et al., 2002; IPCC, 2013; Penner et al., 2004). Furthermore, aerosols have been shown to alter regional precipitation patterns (Menon et al., 2002) and reduce visibility (Che et al., 2007; Jia, 2011; Zhu et al., 2015).

With the unprecedented economic growth, population expansion and urbanization over the past two decades, China has become one of the world's most polluted regions (Li et al., 2007; Duncan et al., 2003), particularly regions in Northern China (Cao et al., 2012; Zhang et al., 2013). Aerosol optical properties in Northern China have been extensively researched (Che et al., 2007; Cheng et al., 2008; He et al., 2009). For example, Jing et al. (2015) in an urban site Beijing and Yan et al. (2008) in a rural site Shangdianzi analyzed diurnal cycles and seasonal variations of aerosol optical properties based on long-term measurement, both observing aerosol scattering coefficients and absorption coefficients had a similar diurnal cycle with a maximum at night and a minimum in the afternoon while ω presented an opposite diurnal

* Corresponding author at: Environment Research Institute, Shandong University, Jinan 250100, China.
E-mail address: yanglingxiao@sdu.edu.cn (L. Yang).

http://dx.doi.org/10.1016/j.atmosres.2016.12.011
0169-8095/

variation and the seasonal variations with highest scattering coefficients in autumn. Some works have focused on the relationship between optical properties and trace gases (Li et al., 2007) or chemical composition (Tao et al., 2016; Li et al., 2013). It was found that mobile sources significantly influence aerosol optical properties and that $(NH_4)_2SO_4$ and NH_4NO_3 were the dominant contributors to the total extinction (σ_{ext}, the sum of σ_{sp} and σ_{ap}) under dry conditions. Deeply, aimed at investigating some special events, many measurements were conducted. Jung et al. (2009) and Garland et al. (2009) both investigated the aerosol optical properties during Campaign of Air Quality Research in Beijing 2006 (CAREBeijing-2006) and found low wind speeds from south exacerbated haze episodes in Beijing. Additionally, Ma et al. (2011) reported that the maximum σ_{sp} and σ_{ap} occurred under southerly winds due to the pollutants transport from southern polluted areas through investigating aerosol optical and physical properties at a town Wuqing; Yu et al. (2013) found the average aerosol optical depth coupled with the lowest Ångström exponent during dust episodes was largest among the three different pollution episodes (fire work, biomass burning and dust episodes) that occurred in Beijing. And also in Beijing, Che et al. (2007) obtained the ω values at 500 nm for clean, haze, and dust days were 0.88, 0.86, and 0.93 respectively, which indicated that haze aerosols had more absorption ability than mineral aerosols on the dusty day.

Numerous aerosol optical properties studies conducted in Northern China have focused on the Beijing-Tianjin-Hebei (Jing-Jin-Ji) region, while little attention has been given to the Shandong Province, which is the other severely polluted region in Northern China and has been already included in the Chinese national plan for regional air pollution control (Cheng et al., 2011; Wang and Hao, 2012). Many analyses from the Jing-Jin-Ji region have been carried out based on measurement at one single site, but measurement of aerosol optical properties in different sites, especially one urban site and one background site, were rarely reported. It has been demonstrated that aerosol can significantly alter the earth's radiation budget; however, the degree and direction of influence varies by location and aerosol optical depth and composition, which makes estimating aerosol forcing difficulty (Dubovik et al., 2002; Shi et al., 2013). It is necessary have adequate information on aerosol temporal and spatial distributions, chemical composition, and their associated properties across the globe to decrease uncertainty in radiative balance estimates (Pilinis et al., 1995; Ramaswamy et al., 2001; Lyamani et al., 2010). By obtaining measurements from one urban and one coastal site, we discussed and compared their seasonal and diurnal characteristics, wind dependency of σ_{sp}, σ_{ap} and ω. Therefore results obtained from our study are of special importance for all researchers interested in investigating the role of aerosols prevalent over this region on regional-scale radiative forcing and their possible global impacts.

Previous studies in Shandong Province have mainly focused on chemical components of aerosols pollution (Liu et al., 2016; Gu et al., 2014; Zhang et al., 2014; Yang et al., 2012; Gao et al., 2011; Cheng et al., 2011). Shandong Province emits the largest amount of air pollutant (SO_2, NOx and PM) in the country and in the world, which are important precursors for the scattering aerosol species such as sulphate and nitrate (Zhang et al., 2009). Furthermore, it has been demonstrated that long-range aerosol transport from the Shandong Province could play an important role for the haze episode in the Jing-Jin-Ji region (Kong et al., 2010; Jung et al., 2009). Therefore, investigating aerosol optical properties in Shandong Province is also beneficial for better understanding regional pollution in Northern China.

In this paper, we present the aerosol optical properties (e.g., scattering coefficients, absorption coefficients and single-scattering albedo) measured at the urban site of Jinan from 1 December 2013 to 30 May 2014 (winter: December 2013 to February 2014; spring: March to May 2014) and the coastal site of Tuoji Island from 9 December 2014 to 12 January 2015. Distinct characteristics between the urban site and coastal site are discussed and the diurnal characteristics and wind dependency of these optical parameters are analyzed.

2. Measurement

2.1. Field site

The city of Jinan (36.67° N, 117° 02′ 01″ 117.05° E) is situated in the north-central Shandong Province (Fig. 1). The measurement site was located on the rooftop of the teaching building at Shandong University, which is approximately 20 m above ground. The instruments were installed in a temperature controlled room, which was maintained at 21 °C. The sample air was collected by a stainless steel tube with a diameter of about 1.9 cm located 5 m above ground level.

The coastal site of Tuoji Island (38.19° N, 120.74° E) is located on the eastern coastal part of the Shandong Province (Fig. 1). Measurements were obtained at the Tuoji Island station, which is one of the regional Global Atmosphere Watch stations in China. The instruments were installed in an air-conditioned room on the third floor, and the sample flow passed through stainless steel tubing (1.9 cm, 5 m) on the rooftop, located 4 m above ground level.

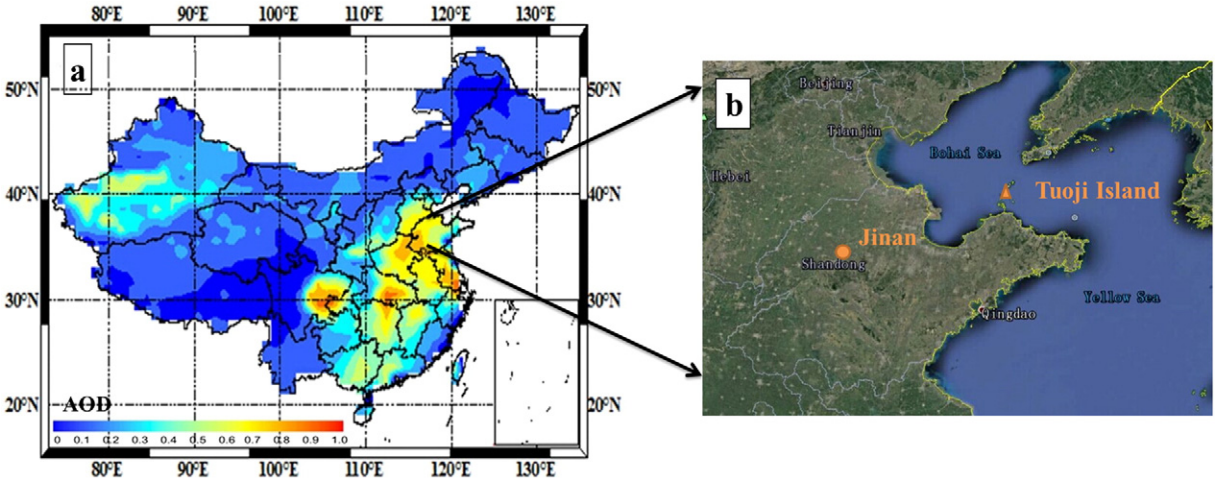

Fig. 1. Map showing the study area (a) the aerosol optical depth in China during 1985–2014 years (http://www.radi.cas.cn/dtxw/rdxw/125xmp2/201608/t20160829_4656117.html) and (b) the location of our sampling sites (an orange circle: Jinan; an orange triangle: Tuoji Island).

2.2. Instrumentation

Aerosol total scattering coefficients (σ_{sp}) were measured by a high-sensitivity, total-scatter integrating nephelometer at 450, 550 and 700 nm (Model 3563, TSI, USA). This instrument was equipped with an inlet with two temperature sensors, one relative humidity sensor, and a pressure sensor, and a halogen lamp as the light source. When the ambient air was drawn into chamber, the instrument measured scattered light at the wavelength of 450, 550 and 700 nm using three photomultiplier tubes at 5-minute intervals. The nephelometer was calibrated every 3 months, with filtered air (low-span gas) and CO_2 (high-span gas) gas as described in the instrument's manual. The zero signal was measured hourly. In the case of relative humidity (RH) < 50%, the scattering coefficient has a slight dependence on RH. However, when RH exceeds 80%, there exists a sharp correlation increase between the scattering coefficient and RH (Anderson and Ogren, 1998; Xu et al., 2002). In this study, the RH measured within the nephelometer chamber was maintained below 50% RH, therefore, the light scattering measurements were considered to be dry.

The mass concentrations of black carbon were obtained with an aethalometer (Model AE21, Magee Scientific, USA). The filter continuously drew the air samples through the inlet port on the quartz fibre filter, where the aethalometer performed optical attenuation measurement at 370 and 880 nm. Since black carbon is regarded as the sole absorbent of sun light at 880 nm (Hansen et al., 1984; Xu et al., 2012; Tiwari et al., 2015). So the results which recorded at 880 nm wavelength in the present study were exclusively used to determine BC concentration (Xu et al., 2012). The data of black carbon mass concentrations were provided in unit of μg/m^3. The aethalometer was placed in air-conditioned rooms which were mentioned in Section 2.1, and RH of the rooms was maintained between 40 and 50%. The flow rate of the aethalometer was maintained at 5 L/min.

Particles size distribution data (5 nm–10 μm) were measured with a high-resolution aerosol spectrometer (WPS model1000XP; MSP Corporation, USA). This instrument comprised of a differential mobility analyzer (DMA), a condensation particle counter (CPC) and a laser particle spectrometer (LPS). The particle number concentration between 5 and 500 nm was measured by DMA and CPC, and the LPS determined the particle concentration in the 350–10,000 nm ranges. Additional details on the operational and calibration methods can be found in Gao et al. (2007).

Meteorological parameters such as wind speed, wind direction, RH and temperature were obtained from an automatic weather station (CAWS600, China Huayun Group) in Jinan and a portable automatic weather station (NK4500, Kestrel, USA) on Tuoji Island. A portion of temperature data on Tuoji Island is missing due to the instrument error.

2.3. Data processing

The single-scattering albedo (ω), at a given wavelength λ is determined by the following:

$$\omega(\lambda) = \frac{\sigma_{sp}(\lambda)}{\sigma_{ap}(\lambda) + \sigma_{sp}(\lambda)} \quad (1)$$

where σ_{ap} (λ) is the particle absorption coefficient, and σ_{sp} (λ) is the particle scattering coefficient. In our work, we calculated the hourly ω values from Eq. (1) by using the σ_{sp} at 532 nm obtained with the nephelometer and the σ_{ap} at 532 nm gained with the aethalometer. The σ_{ap} at 532 nm was calculated by the following:

$$\sigma_{ap} = 8.28 \times [BC] + 2.23 \quad R^2 = 0.92 \quad (2)$$

where [*BC*] is the mass concentration of BC (μg/m^3), and the value 8.28 is the conversion factor in m^2/g (Hansen, 2005). This equation has been previously utilized by He et al. (2009) in the urban site in Beijing and Tiwari et al. (2015) in the urban city Delhi. Considering the three urban sites are typical cities in Asia, Especially, Beijing and Jinan are both inland cities in Northern China and they both are severely polluted area, so we also use this equation to calculate the absorption coefficient at a wavelength of 532 nm.

The σ_{sp} at 532 nm was calculated using the following equation:

$$\mathring{a}_s(\lambda_1/\lambda_2) = -\frac{log\left(\sigma_{s,\lambda_1}/\sigma_{s_{,\lambda_2}}\right)}{log(\lambda_1/\lambda_2)} \quad (3)$$

with the inputs, $\mathring{a}_s = \mathring{a}_s$ (550/700) $\sigma_{sp,\lambda 1} = \sigma_{sp,550}$ and with $\lambda_1 =$ 550 nm and $\lambda_2 =$ 532 nm (Garland et al., 2008).

3. Results and discussion

3.1. Overview of aerosol optical properties

3.1.1. Overview

The measured aerosol optical properties in Jinan and Tuoji Island are summarised in Table 1. There existed some seasonal differences in the aerosol optical properties in Jinan. During the winter campaign, the average σ_{sp} (550 nm) was 315 ± 208 Mm^{-1}, which ranged between 47 and 1074 Mm^{-1}, whereas the average scattering coefficient was 119 ± 89 Mm^{-1} in the spring campaign, which exhibited a narrower range of 18 to 428 Mm^{-1}. The aerosol absorption coefficient exhibited a similar seasonal variation. The average aerosol absorption coefficient was larger in the winter (63 ± 44 Mm^{-1}) than in the spring (30 ± 13 Mm^{-1}), indicating larger near-surface aerosol loading during the winter than in spring (Lyamani et al., 2010). The winter mean aerosol scattering coefficient was 2.6 times larger than average values observed in the spring and the winter mean aerosol absorption coefficient was greater than measurements obtained in spring by a factor of 2.1. This reveals that the loading of scattering aerosols was more enhanced than absorbing aerosols in the winter. Furthermore, the standard deviations of σ_{sp} and σ_{ap} during the winter were larger than springtime measurements, which indicates significant day-to-day aerosol scattering and absorption coefficients variability during the winter (Lyamani et al., 2010). This is discussed in greater details in Section 3.2. The average ω at the wavelength of 532 nm in Jinan was 0.84 ± 0.05 and 0.77 ± 0.09 in winter and spring, respectively. The higher ω (532 nm) values observed during the winter indicate an increased fraction of scattering particles during this time.

Table 1
Summary of seasonal average aerosol optical properties (mean, standard deviation and range of σ_{sp}, σ_{ap} and ω) in Jinan and Tuoji Island.

Site		Jinan						Tuoji Island		
		Mean		Std		Range		Mean	Std	Range
Parameters	λ	Winter	Spring	Winter	Spring	Winter	Spring	Winter	Winter	Winter
σ_{sp} (Mm^{-1})	450 nm	432	166	280	120	58–1462	25–582	304	350	22–1336
	550 nm	315	119	208	89	47–1074	18–428	210	246	16–942
	700 nm	210	77	141	60	33–717	12–290	126	148	11–572
σ_{ap} (Mm^{-1})	532 nm	63	30	44	13	11–214	11–65	8	6	3–24
ω	532 nm	0.84	0.77	0.05	0.09	0.64–0.92	0.53–1.05	0.93	0.04	0.85–0.98

On Tuoji Island, the average value of σ_{sp} (550 nm) was 210 ± 246 Mm^{-1}, which was lower than that in Jinan (315 ± 208 Mm^{-1}) during winter. Interestingly, the σ_{ap} was substantially low, with an average of 8 ± 6 Mm^{-1}, which demonstrated the low concentration of absorbing particles. Tuoji Island is surrounded by the sea, has no large-scale industries, and only a small number of vehicles, which resulted in a particularly low σ_{ap} value. The average ω value of 0.93 further confirmed that the particle type in this region is dominated by scattering particles.

3.1.2. Comparison with other sites

The campaign-averaged σ_{sp} (550 nm) and σ_{ap} (532 nm) in Jinan during December 2013–May 2014 were 204 ± 188 Mm^{-1} and 43 ± 33 Mm^{-1}, respectively (Table 2). Compared with other urban sites in Northern China, these values were lower than measurements obtained in Beijing (He et al., 2009; Wu et al., 2014) and in Xi'an (Zhu et al., 2015). However, the mean values in Jinan were larger than the values from many urban areas in southern China, e.g., Guangzhou (Garland et al., 2008), Nanjing (Zhuang et al., 2014), and Hong Kong (Gao et al., 2015). In addition, the mean values of σ_{sp} and σ_{ap} were higher than in other cities outside of China, such as Granada in Spain (Lyamani et al., 2010) and Atlanta in the United States (Greenwald et al., 2007).

The mean σ_{sp} values on Tuoji Island were lower than those in most urban cities in northern China but higher than those in urban and rural sites in southern China. However, the σ_{ap} values measured on Tuoji Island were nearly the lowest among these sites in Table 2.

Compared to the other campaigns (particularly those in China) listed in Table 2, the ω values observed in Jinan were the lowest, indicating the percent of darker (i.e., more absorbing) aerosols and a higher relative abundance of light-absorbing carbon and combustion aerosols (Ma et al., 2011; Lyamani et al., 2010). The ω values obtained on Tuoji Island were fairly great compared to the other measurement sites.

3.2. Diurnal cycles

The diurnal variations of σ_{sp} (550 nm), σ_{ap} (532 nm), ω, wind speed and temperature averaged over all data available in Jinan during winter and spring and on Tuoji Island in winter are exhibited Fig. 2. The diurnal patterns of σ_{sp} and σ_{ap} in Jinan were similar in winter and spring, with two maxima and minima within a day (Fig. 2a and b). The values of σ_{sp} and σ_{ap} reached a maximum in the morning between 0800 and 1100 LT. During this period, the rapid increase of scattering and absorbing aerosol was likely due to the increased emissions from traffic during the morning rush hours. This was exacerbated by the low boundary layer that facilitated particle accumulation near the surface (Navas-Guzmán et al., 2007) and therefore resulted in greater σ_{sp} and σ_{ap}. After this period, both σ_{sp} and σ_{ap} slowly decreased and the lowest values were observed in the afternoon around 1500 to 1600 LT. This phenomenon can be attributed to the gradual increase in solar heating, convective activity and decreased anthropogenic emissions. Furthermore, the gradually increasing wind speeds (Fig. 2a and b) during this period accelerated the diffusion of aerosols in the atmosphere (He et al., 2009).

Table 2
Aerosol particle scattering coefficients, absorption coefficients and single-scattering albedo values observed in this study and as reported for other selected campaigns (arithm. mean ± std. dev.).

Site	Type	Period	σ_{sp} (Mm^{-1})	σ_{ap} (Mm^{-1})	ω	Instrumentation	Reference
Jinan, China	Urban	2013.12–2014.5	204 ± 188 (550 nm)	43 ± 33 (532 nm)	0.80 ± 0.09 (532 nm)	AE21[a] Nephelometer[b]	Our work
Tuoji Island, China	Coastal	2014.12.6–2015.1.12	210 ± 246 (550 nm)	8 ± 6 (532 nm)	0.93 ± 0.04 (532 nm)	AE21[a] Nephelometer[b]	Our work
Beijing, China	Urban	2009.6–2010.5	360 ± 405 (525 nm)	64 ± 62 (525 nm)	0.82 ± 0.09 (525 nm)	AE31[c] Nephelometer[d]	Wu et al. (2014)
Beijing, China	Urban	2005.1–2006.12	288 ± 281 (525 nm)	56 ± 49 (532 nm)	0.8 ± 0.09 (525 nm)	AE16[e] Nephelometer[f]	He et al. (2009)
Xi'an, China	Urban	2012.8–10	270 ± 201 (532 nm)	31 ± 28 (532 nm)	0.88 ± 0.09 (532 nm)	Photoacoustic Extinctiometers[g]	Zhu et al. (2015)
Guangzhou, China	Urban	2006.7	151 ± 103 (550 nm)	34.3 ± 26.3 (532 nm)	0.86 ± 0.07 (532 nm)	PAS[h] Nephelometer[b]	Garland et al. (2008)
Nanjing, China	Urban	2011.1.18–4.18	170.9 ± 105.8 (550 nm)	4.1 ± 2.2 (550 nm)	/	AE31[c] Nephelometer[i]	Zhuang et al. (2014)
Hong Kong, China	Urban	2010.10–12	201.96 ± 105.82 (532 nm)	39.91 ± 19.16 (532 nm)	0.82 ± 0.07 (532 nm)	AE31[c] Nephelometer[b]	Gao et al. (2015)
Wuqing, China	Rural	2009.3.6–4.5	280 ± 253 (550 nm)	47 ± 38 (637 nm)	0.82 ± 0.05 (532 nm)	MAAP[j] Nephelometer[b]	Ma et al. (2011)
SDZ, China	Rural	2003.09–2005.01	174.6 ± 189.1 (525 nm)	17.54 ± 13.44 (525 nm)	0.88 ± 0.05	AE31[c] Nephelometer[f]	Yan et al. (2008)
Yulin, China	Rural	2001.3.30–5.1	158 ± 193 (530 nm)	6 ± 11 (565 nm)	0.95 ± 0.05 (532 nm)	PSAP[k] Nephelometer[l]	Xu et al. (2004)
Granada, Spain	Urban	2005.12–2007.11	60 ± 30 (550 nm)	21 ± 10 (670 nm)	0.68 ± 0.07 (670 nm)	MAAP[m] Nephelometer[b]	Lyamani et al. (2010)
Atlanta, US	Urban	2004.8	71 ± 36 (550 nm)	6.7 ± 4.8 (567 nm)	0.89 ± 0.06	PSAP[k] Nephelometer[l]	Greenwald et al. (2007)

[a] Aethalometer (Model AE21, Magee Scientific Co., USA).
[b] Integrating Nephelometer (Model 3563, TSI, Inc., Shoreview, MN USA).
[c] Aethalometer (Model AE31, Magee Scientific Co., USA).
[d] Integrating Nephelometer (Aurora-1000, Ecotech Pty Ltd., Australia).
[e] Aethalometer (Model AE16, Magee Scientific Co., USA).
[f] Integrating Nephelometer (Model M9003, Ecotech, Australia).
[g] Photoacoustic Extinctiometers (PAX, Boulder, CO, USA).
[h] Photoacoustic Spectrometer (PAS, Desert Research Institute).
[i] Integrating Polar Nephelometer (NGN-3A, OPTEC Inc., USA).
[j] Multi-angle Absorption Photometer (MAAP, Model 5012, Thermo, Inc., Waltham, MA, USA).
[k] Particle Soot Absorption Photometer (PSAP, Radiance Research, Seattle, WA).
[l] Radiance Research Nephelometer.
[m] Multi-angle Absorption Photometer (MAAP, Thermo ESM Andersen Instruments, Erlangen, Germany).

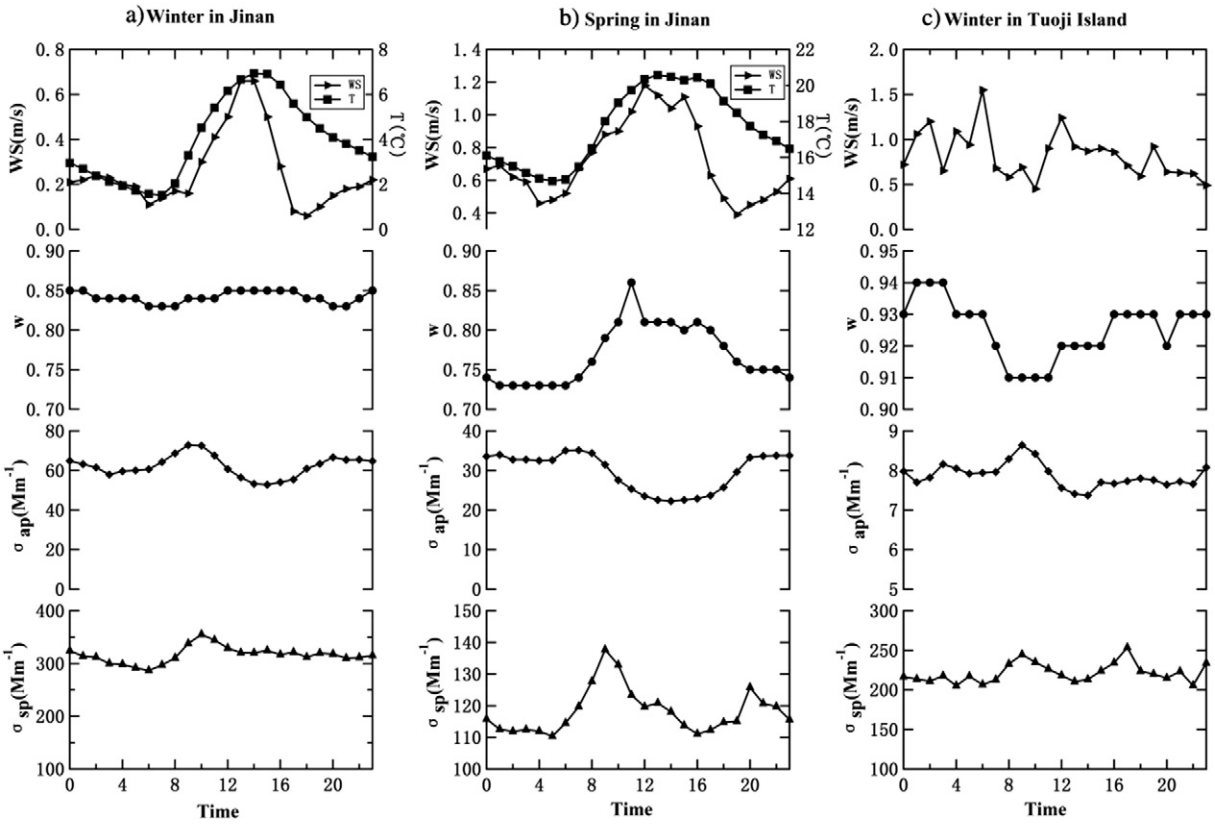

Fig. 2. The average diurnal cycle of σ_{sp}, σ_{ap}, ω, wind speed and temperature: (a) winter in Jinan; (b) spring in Jinan; (c) winter on Tuoji Island.

In the evening, the values increased and reached their secondary peaks around 1900 to 2100 LT. The increase in σ_{sp} and σ_{ap} late in the evening was due to the evening traffic peak and a decrease in both the boundary layer height and wind speed. After 2300 LT, the values of σ_{sp} and σ_{ap} gradually decreased and the second minimum was reached at night between 0400 and 0500 LT.

The ω diurnal pattern in the spring exhibited one maximum that occurred between 1000 and 1400 LT (Fig. 2b). It has been previously shown that an increase in temperature and light intensity enhanced the light-scattering potential of aerosols through secondary aerosol formation and aging processes (Wiedensohler et al., 2009; Wu et al., 1990; Yan et al., 2008), which may explain the ω peak in the afternoon. There was not a discernible ω diurnal pattern during the winter months due to the cool temperature and weak solar heating.

The diurnal cycle on Tuoji Island was similar to that observed in Jinan, with two maxima and two minima (maxima: 0800 to 1000 LT and 1600 to 1800 LT; minima: 1200 to 1400 LT and 2100 to 2300 LT), but the peaks were less prominent (Fig. 2c). This pattern reflects the increase in the number of motor vehicles observed during the peak traffic times. Similar to vehicular traffic, there is increased sailing between the island and mainland between 0800 to 0900 LT and 1400 to 1700 LT, which likely contributed to the variation in the optical properties.

As can be seen from the graph in Fig. 2c, ω values were frequently above 0.9, and scattering particles were dominant on the island. When the absorption coefficient and scattering coefficient concurrently reached a maximum, ω values exhibited a decreasing trend, which suggests that traffic sources contributed more to the absorption coefficient than to the scattering coefficient.

3.3. Relationship with wind direction and wind speed

To understand the function of wind direction on σ_{sp} and σ_{ap}, we combined σ_{sp} and σ_{ap} with the wind direction in a rose plot. Fig. 3 shows the wind direction frequency and the mean σ_{sp} and σ_{ap}. We also determined wind speeds that were typically observed during period of high σ_{sp} and σ_{ap} values for the major wind directions, which are exhibited in Fig. 4.

In Jinan, the winds most frequently were from the northeast and southwest in the winter, while the dominant wind direction was from the southwest in Tuoji Island during the winter (Fig. 3). The σ_{sp} and σ_{ap} values observed in Jinan during winds from 225° to 270° were mostly low, while the high σ_{sp} (>800 Mm^{-1}) and σ_{ap} (>180 Mm^{-1})values were mostly observed under winds from 0° to 90° (Fig. 3a and b). The high σ_{sp} and σ_{ap} values from 0° to 90° were always accompanied by calm winds (0 to 2 m/s) (Fig. 4a). This indicates that local sources from the region between 0° to 90° largely influence the σ_{sp} and σ_{ap} values (Gao et al., 2011; Cheng et al., 2011). In the winter on the Tuoji Island, a majority of σ_{sp} and σ_{ap} values were clustered in the region from 180° to 270° (Fig. 3e and f). The region with high σ_{sp} values (>800 Mm^{-1}) at intermediate and high wind speeds (>2 m/s) comprises above 80% of the total high σ_{sp} value, in which the σ_{sp} high values accompanied by high wind speed (>4 m/s) taking up 30% of the total high σ_{sp} value. And the high σ_{ap} values (30 to 40 Mm^{-1}) from this region occurred when the wind speed totally exceeded 2 m/s (Fig. 4c). This indicates that regional middle- and long-distance transport from Shandong Province likely produced the high σ_{sp} and σ_{ap} values on the Tuoji Island (Zhang et al., 2016; Feng et al., 2007). Noticeably, when the winds were from 270° to 315° at high wind speed (>4 m/s, long-distance transport), the σ_{sp} values were always high (>800 Mm^{-1}) (Fig. 3e and f). Thus, even though the wind from 270° to 315° occupied only a small region, long-distance transport from Jing-Jin-Ji region can have a significant effect on σ_{sp} values on Tuoji Island (Zhang et al., 2016; Feng et al., 2007). Furthermore when the wind came from 45° to 90° at high speed (>4 m/s), the σ_{ap} values were very low (<10 Mm^{-1}), which suggests that the regional transport from 45° to 90° provided a clean air mass (marine air mass) that enhanced the diffusion of

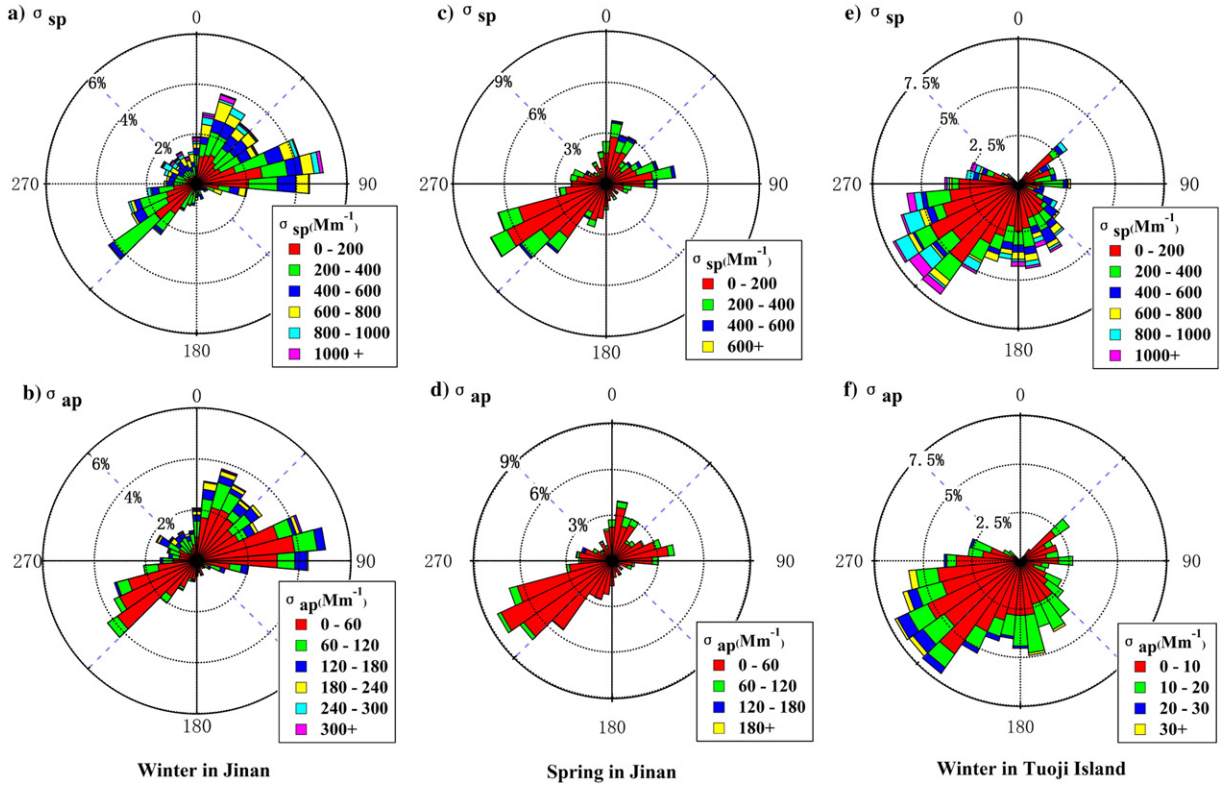

Fig. 3. Frequency plot of total σ_{ap} and σ_{sp} in Jinan and Tuoji Island as a function of wind direction. Each bar of the frequency plot represents 10°. The magnitude of the bars indicates the wind direction frequency, and the colour of the bars shows the value of σ_{ap} and σ_{sp} for a given wind direction (1-h means).

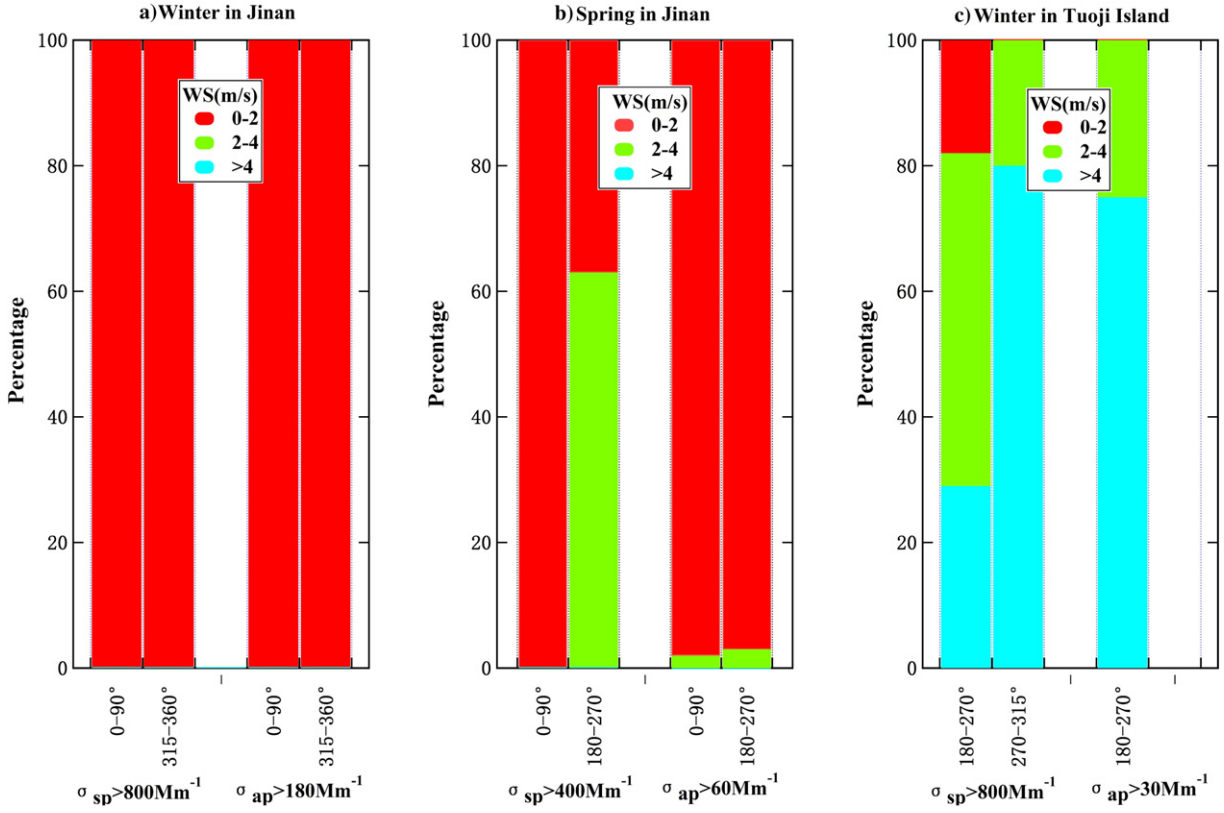

Fig. 4. The percentage of wind speed in the directions with high σ_{sp} and σ_{ap} values: (a) winter in Jinan, (b) spring in Jinan and (c) winter on Tuoji Island.

pollutants (Feng et al., 2007). The differences in the aerosol optical properties between the winter of Jinan and Tuoji Island can be explained by two main reasons: First, most of the large-scale industries, such as heat-engine plants and the power station, are located in the northeast Jinan, which could lead to abundant emissions of aerosols during the winter heating period. Therefore, when the wind came from 0° to 90° at low wind speeds (0 to 2 m/s), the σ_{ap} and σ_{sp} values were levated, which corresponded period of severe air pollution. Secondly, there are no large-scale industries on Tuoji Island. From our analyses, it can be concluded that the high σ_{sp} and σ_{ap} values measured on Tuoji Island were mainly due to the influence of regional middle- and long-distance transport from Shandong Province and Jing-Jin-Ji region.

During the spring portion of the Jinan campaign (Fig. 3c and d), the σ_{sp} and σ_{ap} values were still dominantly concentrated in the directions from 0° to 90° and 180° to 270°, with the wind from 180° to 270° accounting for a greater portion. The high σ_{sp} (>400 Mm^{-1}) and σ_{ap} (>60 Mm^{-1}) values observed in spring were less than those (σ_{sp} > 800 Mm^{-1} and σ_{ap} > 180 Mm^{-1}) in winter. The high σ_{sp} and σ_{ap} values occurred during wind from 0° to 90° with low wind speeds (0 to 2 m/s), which is indicative of local emissions (Fig. 4b). The time at which the high σ_{sp} and σ_{ap} values occurred was close to the end but still within the period of heating. High σ_{sp} values were also occasionally measured when the wind came from 180° to 270° at intermediate wind speeds (2 to 4 m/s) after the heating period, which indicates that middle- and long-distance regional transport from this direction also had a certain effect on air pollution in spring.

3.4. Relationship with particle concentration and size distribution

The σ_{sp} as a function of the particle number concentration in different modes in Jinan and Tuoji Island is displayed in Figs. 5 and 6. We classified particle with diameters of 5 to 20 nm as nucleation mode, 20 to 100 nm as Aiken mode and 100 to 1000 nm as accumulation mode (Yuan et al., 2014). The relationship between σ_{sp} and different modes particle number concentration in Jinan is similar with that on Tuoji Island (Figs. 5 and 6). The σ_{sp} clearly correlated with the number concentration of accumulation mode particles (Jinan: $R^2 = 0.40$; Tuoji Island: $R^2 = 0.64$), indicating that aerosol particles in the accumulation mode have the highest scattering efficiency at the measured wavelengths (Figs. 5 and 6) (Aaltonen et al., 2006). No clear relationship was found between σ_{sp} and the particle number concentrations with the other modes, including nucleation mode, Aiken mode and total particles.

4. Conclusions

In this study, we investigated aerosol optical properties in the urban area of Jinan from December 2013 to May 2014 (winter: December 2013 to February 2014; spring: March to May 2014) and the coastal site of Tuoji Island from 9 December 2014 to 12 January 2015. The average σ_{sp} (550 nm) and σ_{ap} (532 nm) in Jinan from the full measurement period were 204 ± 188 Mm^{-1} and 43 ± 33 Mm^{-1}, respectively, and the average σ_{sp} and σ_{ap} values on Tuoji Island during the winter measurement were 210 ± 246 Mm^{-1} and 8 ± 6 Mm^{-1}, respectively.

Pronounced and distinctive diurnal cycles of the aerosol optical parameters were found between Jinan and Tuoji Island. The σ_{sp} and σ_{ap} exhibited the greatest values between 0800 LT and 1100 LT in the morning and around 1900 to 2100 LT in the evening in Jinan winter, which was mainly affected by a result of the coupling of increasing traffic emission and with low wind speed. A unimodal diurnal pattern of ω was observed, which peaked between 1000 and 1400 LT in Jinan in the spring. This diurnal pattern was mainly related to secondary aerosol formation and aging processes.

The wind speed and direction strongly affected the aerosol optical properties at both locations. The high σ_{sp} and σ_{ap} values in Jinan were

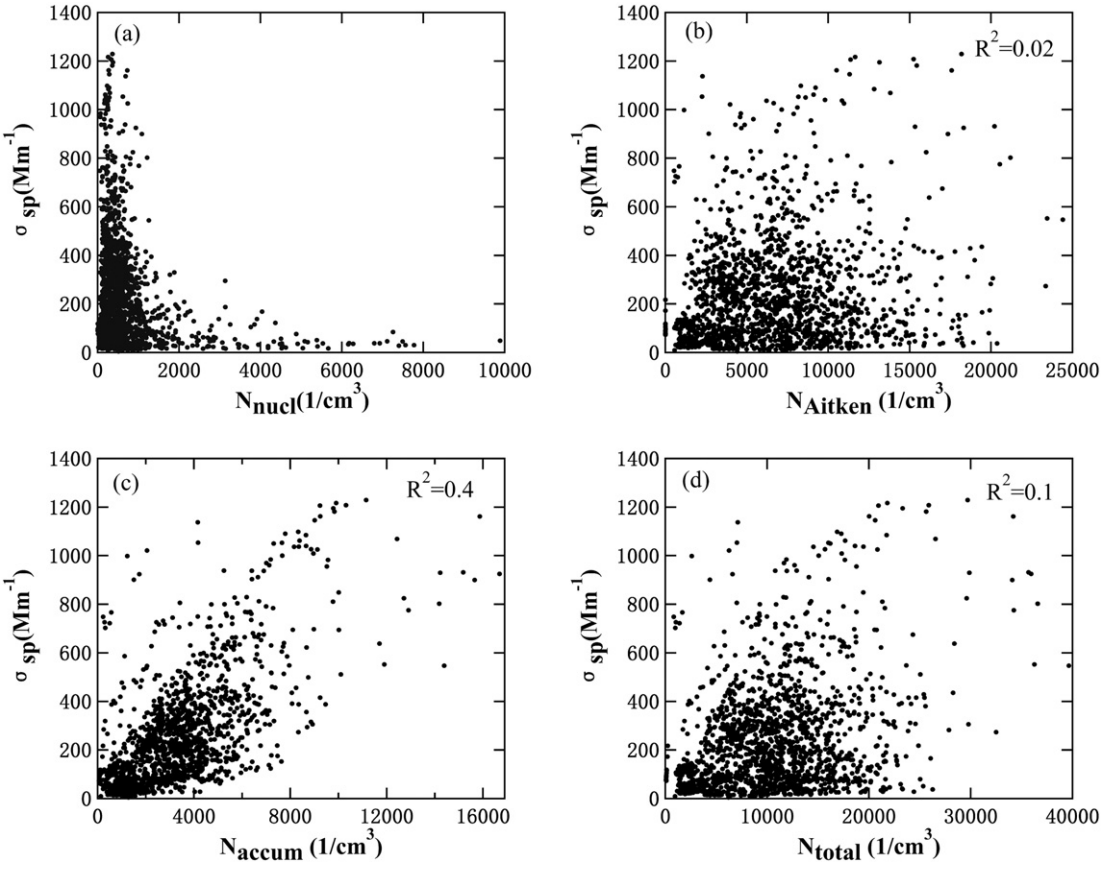

Fig. 5. Relationship between σ_{sp} at 550 nm and (a) nucleation mode, (b) Aiken mode, (c) accumulation mode and (d) total particle number concentration in Jinan.

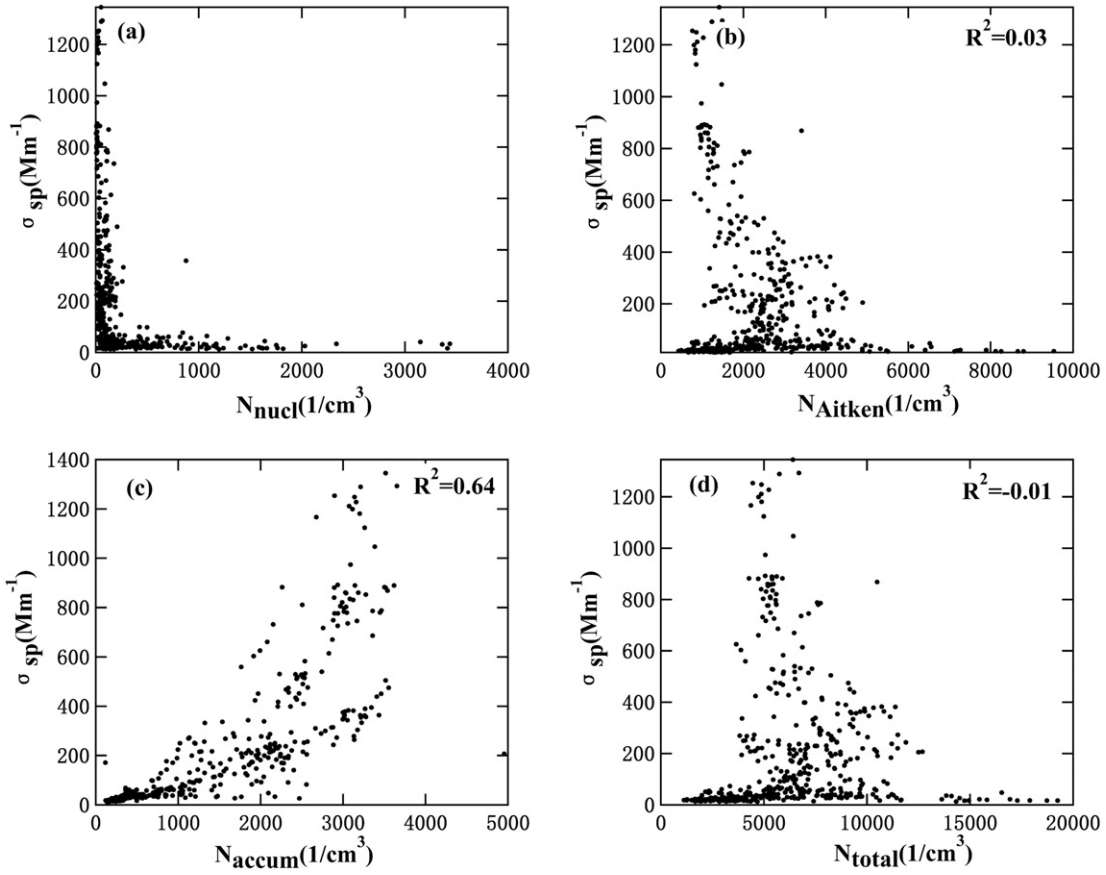

Fig. 6. Relationship between σ_{sp} at 550 nm and (a) nucleation mode, (b) Aiken mode, (c) accumulation mode and (d) total particle number concentration on Tuoji Island.

accompanied by calm winds (0 to 2 m/s) from 0° to 90°, while the high σ_{sp} and σ_{ap} values on Tuoji Island were observed with high wind speed (>2 m/s) from 180° to 270°. This indicated that local emissions during heating period in Jinan winter were a key factor affecting high σ_{sp} and σ_{ap} values, while the high σ_{sp} and σ_{ap} values on Tuoji Island were mainly a result of regional middle- and long-distance transport from Shandong Province and Jing-Jin-Ji region. It was also found middle- and long-distance regional transport from 180° to 270° occasionally had a notable effect on aerosol optical properties after heating period in the springtime in Jinan.

The σ_{sp} values measured at both Jinan and Tuoji Island exhibited a profound correlation with the number concentration of accumulation mode particles, whereas, no clear relationship could be found between σ_{sp} and the particle number concentrations of the other modes (e.g., nucleation mode, Aiken mode and total particles).

Acknowledgements

The work was supported by the National Natural Science Foundation of China (NSFC) (nos. 21307074, 21577079). The authors thank the staff of the Tuoji Island Station for their cooperation during the measurement period.

References

Aaltonen, V., Lihavainen, H., Kerminen, V.-M., Komppula, M., Hatakka, J., Eneroth, K., Kulmala, M., Viisanen, Y., 2006. Measurements of optical properties of atmospheric aerosols in Northern Finland. Atmos. Chem. Phys. 5, 11703–11728.

Anderson, T.L., Ogren, J.A., 1998. Determining aerosol radiative properties using the TSI 3563 integrating nephelometer. Aerosol Sci. Technol. 29, 57–69.

Cao, J.J., Shen, Z.X., Chow, J.C., Watson, J.G., Lee, S.C., Tie, X.X., Ho, K.F., Wang, G.H., Han, Y.M., 2012. Winter and summer $PM_{2.5}$ chemical compositions in fourteen Chinese cities. J. Air Waste Manage. Assoc. 62 (10), 1214–1226.

Che, H., Shi, G., Uchiyama, A., Yamazaki, A., 2007. Intercomparison between aerosol optical properties by a PREDE skyradiometer and CIMEL sunphotometer over Beijing, China. Atmos. Chem. Phys. 7, 16023–16053.

Cheng, T., Zhang, R., Han, Z., Fang, W., 2008. Relationship between ground-based particle component and column aerosol optical property in dusty days over Beijing. Geophys. Res. Lett. 35, 288–299.

Cheng, S.H., Yang, L.X., Zhou, X.H., Wang, Z., Zhou, Y., Gao, X.M., Nie, W., Wang, X.F., Xu, P.J., Wang, W.X., 2011. Evaluating $PM_{2.5}$ ionic components and source apportionment in Jinan, China from 2004 to 2008 using trajectory statistical methods. J. Environ. Monit. 13, 1662–1671.

Dubovik, O., Holben, B., Eck, T.F., Smirnov, A., Kaufman, Y.J., King, M.D., Tanré, D., Slutsker, I., 2002. Variability of absorption and optical properties of key aerosol types observed in worldwide locations. J. Atmos. Sci. 59, 590–608.

Duncan, B.N., Martin, R.V., Staudt, A.C., Yevich, R., Logan, J.A., 2003. Interannual and seasonal variability of biomass burning emissions constrained by satellite observations. J. Geophys. Res. 108, 4100.

Feng, J.L., Guo, Z.G., Chan, C.K., Fang, M., 2007. Properties of organic matter in $PM_{2.5}$ at Changdao Island, China—a rural site in the transport path of the Asian continental outflow. Atmos. Environ. 41, 1924–1935.

Forster, P., Ramaswamy, V., Artaxo, P., Berntsen, T., Betts, R., Fahey, D., Haywood, J., Lean, J., Lowe, D., Myhre, G., 2010. Changes in atmospheric constituents and in radiative forcing. The Physical Science Basis, pp. 129–234.

Gao, J., Wang, J., Cheng, S.H., Xue, L.K., Yan, H.Z., Hou, L.J., Jiang, Y.Q., Wang, W.X., 2007. Number concentration and size distributions of submicron particles in Jinan urban area: characteristics in summer and winter. J. Environ. Sci. 19, 1466–1473.

Gao, X.M., Yang, L.X., Cheng, S.H., Gao, R., Zhou, Y., Xue, L.K., Shou, Y.P., Wang, J., Wang, X.F., Nie, W., Xu, P.J., Wang, W.X., 2011. Semi-continuous measurement of water-soluble ions in $PM_{2.5}$ in Jinan, China: temporal variations and source apportionments. Atmos. Environ. 45, 6048–6056.

Gao, Y., Lai, S.C., Lee, S.C., Yau, P.S., Huang, Y., Cheng, Y., Wang, T., Xu, Z., Yuan, C., Zhang, Y.Y., 2015. Optical properties of size-resolved particles at a Hong Kong urban site during winter. Atmos. Res. 155, 1–12.

Garland, R.M., Yang, H., Schmid, O., Rose, D., 2008. Aerosol optical properties in a rural environment near the mega-city Guangzhou, China: implications for regional air pollution and radiative forcing. Atmos. Chem. Phys. 8, 5161–5186.

Garland, R.M., Schmid, O., Nowak, A., Achtert, P., Wiedensohler, A., Gunthe, S.S., Takegawa, N., Kita, K., Kondo, Y., Hu, M., Shao, M., Zeng, L.M., Zhu, T., Andreae, M.O., Pöschl, U., 2009. Aerosol optical properties observed during campaign of air quality research in Beijing 2006 (CAREBeijing-2006): characteristic differences between the inflow and outflow of Beijing city air. J. Geophys. Res. 114, 1065–1066.

Greenwald, R., Bergin, M.H., Weber, R., Sullivan, A., 2007. Size-resolved, real-time measurement of water-insoluble aerosols in metropolitan Atlanta during the summer of 2004. Atmos. Environ. 519–531.

Gu, J.X., Du, S.Y., Han, D.W., Hou, L.J., Yi, J., Xu, J., Liu, G.H., Han, B., Yang, G.W., Bai, Z.P., 2014. Major chemical compositions, possible sources, and mass closure analysis of $PM_{2.5}$ in Jinan, China. Air Qual. Atmos. Health 7, 251–262.

Hansen, A.D.A., 2005. The Aethalameter Handbook. Magee Scientific Company. Berkeley, California USA.

Hansen, A.D., Rosen, H., Novakov, T., 1984. The aethalometer — an instrument for the real-time measurement of optical absorption by aerosol particles. Sci. Total Environ. 36, 191–196.

Haywood, J.M., Shine, K.P., 1997. Multi-spectral calculations of the direct radiative forcing of tropospheric sulphate and soot aerosols using a column model. Q. J. R. Meteorol. Soc. 123, 1907–1930.

He, X., Li, C.C., Lau, A.K.H., Deng, Z.Z., 2009. An intensive study of aerosol optical properties in Beijing urban area. Atmos. Chem. Phys. 9, 8903–8915.

IPCC, 2013. Summary for policymakers. In: Stocker, T.F., Qin, D., Plattner, G.-K., Tignor, M., Allen, S.K., Boschung, J., et al. (Eds.), Climate Change 2014: The Physical Science BasisContribution of Working Group I to the Fifth Assessment Report of the Intergovernmental Panel on Climate Change. Cambridge University Press, Cambridge, UK and New York, NY.

Jia, G., 2011. Visual range trends in the Yangtze River Delta region of China, 1981–2005. J. Air Waste Manage. Assoc. 61, 843–849.

Jing, J.S., Wu, Y.F., Tao, J., Che, H.Z., Xia, X.G., Zhang, X.C., Yan, P., Zhao, D.M., Zhang, L.M., 2015. Observation and analysis of near-surface atmospheric aerosol optical properties in urban Beijing. Particuology 18, 144–154.

Jung, J.S., Lee, H.L., Kim, Y.J., Liu, X.G., Zhang, Y.H., Hu, M., Sugimoto, N.B., 2009. Optical properties of atmospheric aerosols obtained by in situ and remote measurements during 2006 Campaign of Air Quality Research in Beijing (CAREBeijing-2006). J. Geophys. Res. 114, 1065–1066.

Kaufman, Y.J., Tanré, D., Boucher, O., 2002. A satellite view of aerosols in the climate system. Nature 419, 215–223.

Kong, S., Han, B., Bai, Z.P., Chen, L., Shi, J.W., Xu, Z., 2010. Receptor modeling of $PM_{2.5}$, PM_{10} and TSP in different seasons and long-range transport analysis at a coastal site of Tianjin, China. Sci. Total Environ. 408, 4681–4694.

Li, C., Marufu, L.T., Dickerson, R.R., Li, Z., Wen, T., Wang, Y., Wang, P., Chen, H., Stehr, J.W., 2007. In situ measurements of trace gases and aerosol optical properties at a rural site in northern China during East Asian Study of Tropospheric Aerosols: An International Regional Experiment. J. Geophys. Res. 112, 22.

Li, X., He, K., Li, C., Yang, F., Zhao, Q., Ma, Y., Cheng, Y., Ouyang, W., Chen, G., 2013. $PM_{2.5}$ mass, chemical composition, and light extinction before and during the 2008 Beijing Olympics. J. Geophys. Res. 118, 12158–12167.

Liu, B.S., Song, N., Dai, Q.L., Mei, R.B., Sui, B.H., Bi, X.H., Feng, Y.C., 2016. Chemical composition and source apportionment of ambient $PM_{2.5}$ during the non-heating period in Taian, China. Atmos. Res. 170, 23–33.

Lyamani, H., Olmo, F.J., Alados-Arboledas, L., 2010. Physical and optical properties of aerosols over an urban location in Spain: seasonal and diurnal variability. Atmos. Chem. Phys. 10, 239–254.

Ma, N., Zhao, C.S., Nowak, A., Müller, T., Pfeifer, S., Cheng, Y.F., Deng, Z.Z., Liu, P.F., Xu, W.Y., Ran, L., 2011. Aerosol optical properties in the North China Plain during HaChi campaign: an in-situ optical closure study. Atmos. Chem. Phys. 11, 9567–9605.

Menon, S., Hansen, J., Nazarenko, L., Luo, Y., 2002. Climate effects of black carbon aerosols in China and India. Science 297, 2250–2253.

Navas-Guzmán, F., Guerrero-Rascado, J.L., Fernández-Medina, A.B., Adame, J.A., Alados-Arboledas, L., 2007. Mixing layer height determination by lidar and radiosounding data. European Aerosol Conference 2007, Salzburg, Austria, 9–14 September 2007, Cd1, T20A014.

Penner, J.E., Dong, X., Chen, Y., 2004. Observational evidence of a change in radiative forcing due to the indirect aerosol effect. Nature 427, 231–234.

Pilinis, C., Pandis, S.N., Seinfeld, J.H., 1995. Sensitivity of direct climate forcing by atmospheric aerosols to aerosol size and composition. J. Geophys. Res. 100, 739–754.

Ramaswamy, V., et al., 2001. Radiative forcing of climate change. In: Houghton, J.T., et al. (Eds.), Climate Change 2001: The Scientific Basis. Cambridge Univ. Press, New York, pp. 349–416 (chap. 6).

Shi, C., Wang, S., Zhou, R., Li, D., Zhao, H., Liu, R., Li, Z., Zhou, B., 2013. Aerosol optical properties during dust and biomass burning episodes retrieved from sun-photometer over Shanghai. Atmos. Meas. Tech. Discuss. 6, 11011–11054.

Tao, J., Gao, J., Zhang, L.M., Wang, H., Qiu, X.H., Zhang, Z.S., Wu, Y.F., Chai, F.H., Wang, S.L., 2016. Chemical and optical characteristics of atmospheric aerosols in Beijing during the Asia-Pacific Economic Cooperation China 2014. Atmos. Environ. 144, 8–16.

Tiwari, S., Pandithurai, G., Attri, S.D., Srivastava, A.K., Soni, V.K., Bisht, D.S., Anil Kumar, V., Srivastava, M.K., 2015. Aerosol optical properties and their relationship with meteorological parameters during wintertime in Delhi, India. Atmos. Res. 153, 465–479.

Wang, S., Hao, J., 2012. Air quality management in China: issues, challenges, and options. J. Environ. Sci. 24, 2–13.

Wiedensohler, A., Cheng, Y.F., Nowak, A., Wehner, B., Achtert, P., Berghof, M., Birmili, W., Wu, Z.J., Hu, M., Zhu, T., 2009. Rapid aerosol particle growth and increase of cloud condensation nucleus activity by secondary aerosol formation and condensation: a case study for regional air pollution in northeastern China. J. Geophys. Res. 114, 1283–1289.

Wu, Z., Hu, M., Liu, S., Wehner, B., Bauer, S., Andreas, M.B., Wiedensohler, A., Petäjä, T., Dal Maso, M., Kulmala, M., 1990. New particle formation in Beijing, China: statistical analysis of a 1-year data set. CrystEngComm 17, 797–806.

Wu, Y., Tao, J., Che, H.Z., Jing, J.S., Xia, X.G., Zhang, X.C., Yan, P., Zhao, D.M., Zhang, L.M., 2014. Observation and analysis of near-surface atmospheric aerosol optical properties in urban Beijing. Particuology 18, 144–154.

Xu, J., Bergin, M.H., Yu, X., Liu, G., Zhao, J., Carrico, C.M., Baumann, K., 2002. Measurement of aerosol chemical, physical and radiative properties in the Yangtze delta region of China. Atmos. Environ. 36, 161–173.

Xu, J., Bergin, M.H., Greenwald, R., Schauer, J.J., Shafer, M.M., Shafer, M.M., Jaffrezo, J.L., Aymoz, G., 2004. Aerosol chemical, physical, and radiative characteristics near a desert source region of northwest China during ACE-Asia. J. Geophys. Res. 109, 77–83.

Xu, J.W., Jun, T., Zhang, R.J., Cheng, T.T., Leng, C.P., Huang, G.H., Li, X., Zhu, Z.Q., 2012. Measurements of surface aerosol optical properties in winter of Shanghai. Atmos. Res. 109–110, 25–35.

Yan, P., Tang, J., Huang, J., Mao, J.T., Zhou, X.J., Liu, Q., Wang, Z.F., Zhou, H.G., 2008. The measurement of aerosol optical properties at a rural site in Northern China. Atmos. Chem. Phys. 7, 2229–2242.

Yang, L.X., Zhou, X.H., Wang, Z., Zhou, Y., Cheng, S.H., Xu, P.J., Gao, X.M., Nie, W., Wang, X.F., Wang, W.X., 2012. Airborne fine particulate pollution in Jinan, China: concentrations, chemical compositions and influence on visibility impairment. Atmos. Environ. 55, 506–514.

Yu, X.G., Shi, C.Z., Ma, C.Z., Zhu, B., Li, M., Wang, J., Yang, S.Y., Kang, N., 2013. Aerosol optical properties during firework, biomass burning and dust episodes in Beijing. Atmos. Environ. 81, 475–484.

Yuan, Q., Yang, L.X., Dong, C., Yan, C., Meng, C.P., Sui, X., Wang, W.X., 2014. Particle physical characterisation in the Yellow River Delta of Eastern China: number size distribution and new particle formation. Air Qual. Atmos. Health 8, 1–12.

Zhang, Q., Streets, D.G., Carmichael, G.R., He, K.B., Huo, H., Kannari, A., Klimont, Z., Park, I.S., Reddy, S., Fu, J.S., 2009. Asian emissions in 2006 for the NASA INTEX-B mission. Atmos. Chem. Phys. 9, 5131–5153.

Zhang, R.J., Jing, J.S., Tao, J., Hsu, S.C., Wang, G.H., Cao, J.J., Lee, C.S.L., Zhu, L., Chen, Z., Zhao, Y., Shen, Z.X., 2013. Chemical characterization and source apportionment of $PM_{2.5}$ in Beijing: seasonal perspective. Atmos. Chem. Phys. 13 (14), 7053–7074.

Zhang, J.M., Chen, J.M., Yang, L.X., Sui, X., Yao, L., Zheng, L.F., Wen, L., Xu, C.H., Wang, W.X., 2014. Indoor $PM_{2.5}$ and its chemical composition during a heavy haze-fog episode at Jinan, China. Atmos. Environ. 99, 641–649.

Zhang, J.M., Yang, L.X., Mellouki, A.W., Wen, L., Yang, Y.M., Gao, Y., Jiang, P., Li, Y.Y., Wang, W.X., 2016. Chemical characteristics and influence of continental outflow on $PM_{1.0}$, $PM_{2.5}$ and PM_{10} measured at Tuoji island in the Bohai Sea. Sci. Total Environ. 573, 699–706.

Zhu, C.S., Cao, J.J., Ho, K.F., Chen, L.W.A., Huang, R.J., Wang, Y.C., Li, H., Shen, Z.X., Chow, J.C., Watson, J.G., 2015. The optical properties of urban aerosol in northern China: a case study at Xi'an. Atmos. Res. 160, 59–67.

Zhuang, B.L., Wang, T.J., Li, S., Liu, J., Talbot, R., Mao, H.T., Yang, X.Q., Fu, C.B., Yin, C.Q., Zhu, J.L., 2014. Optical properties and radiative forcing of urban aerosols in Nanjing, China. Atmos. Environ. 83, 43–52.